Eigenvalue decomposition method for photon statistics of frequency-filtered fields and its application to quantum dot emitters

Kenji Kamide,[1,*] Satoshi Iwamoto,[1,2] and Yasuhiko Arakawa[1,2]
[1]*Institute for Nano Quantum Information Electronics (NanoQuine), University of Tokyo, Tokyo 153-8505, Japan*
[2]*Institute of Industrial Science, University of Tokyo, Tokyo 153-8505, Japan*
(Received 19 May 2015; published 18 September 2015)

A simple calculation method for photon statistics of frequency-filtered fields is proposed. This method, based on eigenvalue decompositions of superoperators, allows us to study effects on the photon statistics of spectral filtering by various types of filters, such as Gaussian and rectangular filters as well as Lorentzian filters, which is not possible by conventional approaches. As an example, this method is applied to a simulation of quantum dot single-photon emitters, where we found that the efficient choice of the filter types to have pure single photons depends on the excitation conditions, i.e., incoherent or coherent (and resonant) excitations.

DOI: 10.1103/PhysRevA.92.033833 PACS number(s): 42.50.Ar, 42.50.Ct, 42.50.Dv, 78.67.Hc

I. INTRODUCTION

High-quality single-photon (SP) sources, which emit one photon at a time with high purity and high rate, are essential for the realistic and reliable application to quantum information science and technologies [1,2]. As efficient solid-state SP sources, semiconductor quantum dots (QDs) are promising candidate systems in solids and have been attracting attention for a number of advantages: the well-defined quantized states, high controllability in the emission wavelength, high brightness even enhanced by embedding them in nanocavities, the emission-site controllability, and possible current injection operations [3–12].

However, in QD SP emitters, a number of emission lines are typically present due to the multiple transition levels and also to other QDs in a sample, degrading the SP purity. To avoid the degradation, spectral filters (Fig. 1) are usually used for selecting the relevant emission, e.g., an exciton emission, and filter out the spectrally separated irrelevant emissions, such as the biexciton-exciton emission [14] and charged excitons. The role of using a spectral filter is to prevent the detection of irrelevant emissions spectrally separated in the frequency domain. At the same time, due to the frequency-time uncertainty, using narrow spectral filters inevitably widens the detection field in the time domain, leading to degradation in the time resolution and also in the purity of the SP emissions. In this way, the spectral filter modifies the filtered field both in the frequency and time domains, and therefore the filtering effect on the photon statistics (which basically is a multiple-time correlation function given in the time domain) is not so simply understood, especially for quantum emitters.

Theoretical and experimental studies of filtering effects on the photon statistics have recently been attracting attention [15–19]. These studies were triggered by the development in the theoretical treatment, a versatile calculation method proposed by E. del Valle *et al.* [15]. In this method, the spectral filtering process is effectively replaced with the inclusion of probe systems coupling weakly to the system. A great advantage of this method over the former theory [20–22] is that the complication in calculation coming from the time orderings of operators can be avoided, allowing the calculation of higher-order correlation functions ($n \geqslant 3$). However, in this method, the type of spectral filters the method can treat is restricted to Lorentzian filters, since the spectral filter is mimicked by a Lorentzian density of states of a probe system under the Markov decay process. The former analytic, but approximate, approach [21] also treats only Lorentzian filters due to its simplicity. Therefore, the effect of spectral filtering on the photon statistics has been investigated only for Lorentzian filters so far.

In this paper, we propose a simple calculation method that allows for theoretical treatment of a variety of spectral filters in order to deepen the understanding of filter effect on the photon statistics. In Sec. II, we introduce the calculation method based on superoperator eigenvalue decomposition, and find the exact expressions for the second-order correlation function for Gaussian and rectangular filters as well as the Lorentzian filters. Whereas we apply the superoperator eigenvalue decomposition technique to the higher-order correlation functions, it has previously been applied to the calculation of the first-order correlation functions, e.g., in a calculation of the Mössbauer spectra [23]. While our method allows for the treatment of types of filters, it directly treats the operator ordering problem, and thus the difficulty in calculating high-order correlation functions is not removed. In this sense, our method is complementary to the previous theory [15]. In Sec. III, as an example, we show a numerical simulation applied to QD SP emitter systems, where we found the efficient choice of the filter types for purifying the single photons depends on the excitation conditions, i.e., incoherent or coherent (and resonant) excitations.

We note that the effect of the background noise which is not related to the system dynamics is out of the scope of the theoretical framework. Throughout the paper, we set $\hbar = 1$ for simplicity unless otherwise specified.

II. SUPEROPERATOR EIGENVALUE DECOMPOSITION METHOD FOR PHOTON STATISTICS OF FREQUENCY FILTERED FIELDS

A. Definition of the problem

Here, we will define the problems to solve. The system we consider consists of an emitter, a spectral filter, and a

*kamide@iis.u-tokyo.ac.jp

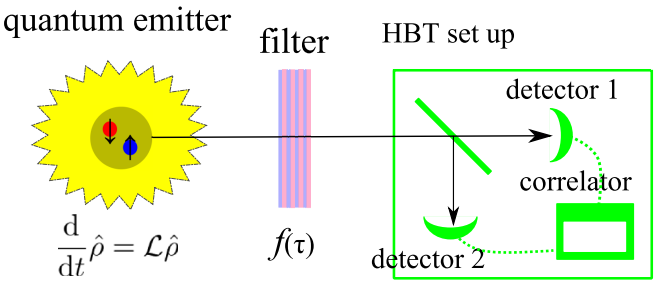

FIG. 1. (Color online) Quantum emitter and detection system. The emission dynamics of the quantum emitter is given by the quantum master equation, $\frac{d}{dt}\hat{\rho} = \mathcal{L}\hat{\rho}$. The effect of the spectral filter is described by the correlation function $f(\tau)$, and the photons passed through the filter enter into the HBT setup [13] for the $g^{(2)}$ correlation measurement.

detection system as shown in Fig. 1. Photons emitted from the quantum emitter are detected by Hanbury-Brown Twiss (HBT) setups [13] for the second-order intensity correlation measurement, and before the detection the photons passed through a spectral filter the response of which is described by the filter correlation function $f(\tau)$. Alternatively, the detection can be performed with a high-speed streak camera with high time resolution (less than a few picoseconds), which is now becoming a powerful detection system for the study of photocounting statistics [24]. Throughout the paper, we assume the effect of back reflection at the filter surface on the emitter system can be neglected [20]. In this case, the dynamics of the quantum emitter and the emission field is given by the Hamiltonian $\hat{H}$ for the emitter, Lindblad-type superoperators $\mathcal{L}_\eta$ for decay and pump processes labeled by η with the rates γ_η, and the resulting quantum master equation [25]:

$$\frac{d}{dt}\hat{\rho} = i[\hat{\rho},\hat{H}] + \sum_\eta \gamma_\eta \mathcal{L}_\eta \hat{\rho} \equiv \mathcal{L}\hat{\rho}. \tag{1}$$

The emission field operator, $\hat{E}^{\pm}$, at the exact emission time, t, is given by the Heisenberg operator (accounting for the system dynamics except for the filter and detection systems), $\hat{E}^{\pm}(t)$, and the frequency-filtered field $\hat{E}_F^{\pm}(t)$ to be detected at a time t is given by

$$\begin{aligned}\hat{E}_F^-(t) &= \int_0^\infty f(\tau)\hat{E}^-(t-\tau)d\tau,\\ \hat{E}_F^+(t) &= \int_0^\infty f^*(\tau)\hat{E}^+(t-\tau)d\tau.\end{aligned} \tag{2}$$

The time region of the integration is physically restricted to $\tau > 0$ by the causality, and the correlation function in the time domain, $f(\tau)$, has the peak at a delay time, $\tau = \tau_d$, corresponding to the optical path length between the emitter and the filter, and it has a width τ_c corresponding to the filter correlation time [Fig. 2(a)]. The filter function $F(\omega)$ in the frequency domain is centered at ω_F and has a bandwidth λ roughly equal to the inverse of the correlation time, $\lambda \sim 1/\tau_c$ [Fig. 2(b)]. Equations (1) and (2) are the most general expression for system dynamics and the filtered emission field, and thus can be directly applied to any emitters and any filters. For example, in case of a resonantly driven two-level

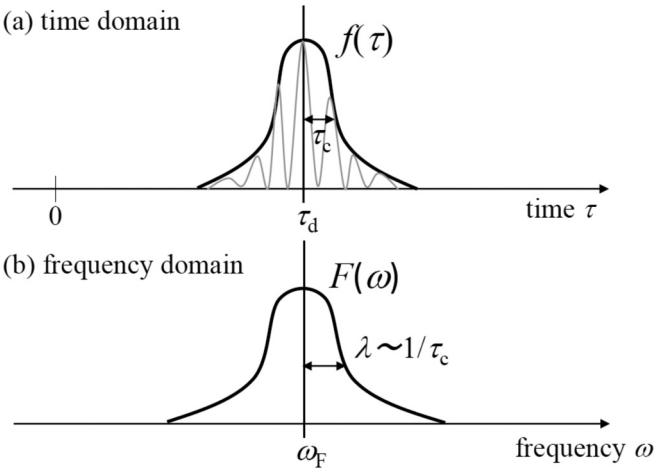

FIG. 2. Schematics of the filter function: (a) $f(\tau)$ in the time domain and (b) $F(\omega)$ in the frequency domain.

atom (transition energy ω_A, Rabi frequency Ω_R, and the laser frequency ω_L), $\hat{H} = \omega_A\hat{\sigma}^+\hat{\sigma}^- + \Omega_R e^{-i\omega_L t}\hat{\sigma}^+ + \Omega_R^* e^{i\omega_L t}\hat{\sigma}^-$, the spontaneous emission decay is included with the rate $\gamma_\eta = \gamma_{sp}$ and superoperator $\mathcal{L}_\eta = \mathcal{L}_{\hat{\sigma}^-}$ in standard notation, and the emission field is $\hat{E}^{\pm}(t) = \hat{\sigma}^{\pm}(t)$.

The nth-order normalized intensity correlation function to be evaluated is then given by

$$\begin{aligned}&g^{(n)}(t_1,t_2,\ldots,t_n)\\ &= \frac{\langle \mathcal{T}_+\mathcal{T}_-\hat{E}_F^+(t_1)\ldots\hat{E}_F^+(t_n)\hat{E}_F^-(t_n)\ldots\hat{E}_F^-(t_1)\rangle}{\prod_{j=1}^n\langle\hat{E}_F^+(t_j)\hat{E}_F^-(t_j)\rangle},\end{aligned} \tag{3}$$

where $\mathcal{T}_-$ and $\mathcal{T}_+$ are time-ordering and antiordering superoperators working on the Heisenberg annihilation and creation operators, respectively. The brackets mean the ensemble statistical average over the emitter states, and mathematically given by taking the trace after multiplying by the density matrix of the emitter system, $\langle\hat{O}\rangle = \mathrm{Tr}(\hat{O}\hat{\rho})$. In addition, from Eq. (2), it is necessary in calculating Eq. (3) to evaluate the operator products with different time arguments by using the quantum regression theorem [25]. The aim of this paper is to give a simple calculation method for the correlation function in Eq. (3).

The time-ordering operation has to be taken into account in Eq. (3) when the effect of back reflection by the filter is negligible as we assumed here [20]. However, the operation makes the calculation of the nth-order correlation function of large n (like $n \geqslant 3$) complicated. For $g^{(n)}(t_1 = \cdots = t_n)$, the number of time arguments (τ_j with $j = 1,\ldots,n$ for $\hat{E}^+$ fields and $j = n+1,\ldots,2n$ for $\hat{E}^-$ fields) is $2n$. The number of different time orderings in the integration is reduced to $(2n)!/(n!)^2$ by a symmetry argument. The number is reduced from $(2n)!$ to $(2n)!/(n!)^2$ since the time-ordering operators $\mathcal{T}_+$ and $\mathcal{T}_-$ sort the product of $\hat{E}^+$ fields and $\hat{E}^-$ fields of $n!$ different orderings, respectively, into one exclusive ordering. Therefore, the number of terms with different time orderings for the nth-order correlation function amounts to 6 for $n = 2$, 20 for $n = 3$, and 70 for $n = 4$ [21].

In our approach given below, we will finally obtain the analytic expression for the correlation function in Eq. (3),

whereas the time-ordering process is directly treated, hence the difficulty is not removed. Therefore, the higher-order correlation function with $n \geqslant 4$ is too computationally expensive. In this sense, this method is limited to the application to the correlation functions with $n \leqslant 3$ in realistic calculation, while the recently proposed method [15] can avoid the complicated time-ordering operation to be able to simulate photon statistics to the higher order.

However, as mentioned in the Introduction, this method allows us to have analytic results for general types of the filter function $f(\tau)$, whereas the previous method [15] can treat only the Lorentzian filters. In this sense, our method is complementary to the other methods [15,21], and this makes possible the comparison of the efficiency in optimizing the photon statistics for different types of filters.

B. Superoperator eigenvalue decomposition method

Here, we will introduce our method based on superoperator eigenvalue decompositions. As an example for $n = 2$, we will obtain a general expression for $g^{(2)}(\tau = t_1 - t_2 = 0)$.

1. Superoperator eigenvalue decomposition

According to the quantum regression formula [25], different-time correlation functions can be calculated by the same equation as the density matrix equation in Eq. (1). Thus, any time-dependent operator $\hat{O}(t)$ satisfies $\frac{d}{dt}\hat{O} = \mathcal{L}\hat{O}$. The matrix equation can be written in a linear equation $\frac{d}{dt}\vec{O} = \mathbf{L}\vec{O}$ after reforming the operator $\hat{O}$ into a vector form $\vec{O} = (\hat{O}_{1,1}, \ldots, \hat{O}_{1,N_c}, \hat{O}_{2,1}, \ldots, \hat{O}_{2,N_c}, \ldots, \hat{O}_{N_c,1}, \ldots, \hat{O}_{N_c,N_c})$. The length of $\vec{O}$ is N_c^2, and the Liouvillian matrix $\mathbf{L}$ (originally the superoperator $\mathcal{L}$) has dimension $N_c^2 \times N_c^2$. Therefore, $\mathbf{L}$ has N_c^2 eigenvalues, Ω, which are in general complex values with $\mathrm{Re}(\Omega) \leqslant 0$. The corresponding right and left eigenvectors, $\vec{v}_\Omega$ and $\vec{u}_\Omega^T$, are defined here as

$$\mathbf{L}\vec{v}_\Omega = \Omega\vec{v}_\Omega, \quad \vec{u}_\Omega^T\mathbf{L} = \vec{u}_\Omega^T\Omega. \tag{4}$$

Therefore, if the eigenvalues are nondegenerate, the operator in vector form, $\vec{O}$, is decomposed into the eigenvectors:

$$\vec{O} = \sum_\Omega C(\Omega)\vec{v}_\Omega, \tag{5}$$

where $C(\Omega) = (\vec{u}_\Omega^T \cdot \vec{O})/(\vec{u}_\Omega^T \cdot \vec{v}_\Omega)$. From the above expression, we obtain the eigenvalue decomposition of the vector by $\vec{O} = \sum_\Omega [\vec{O}]_\Omega$ with $[\vec{O}]_\Omega \equiv C(\Omega)\vec{v}_\Omega$, the matrix form of which with an original Hilbert dimension $(N_c \times N_c)$ is written as $\hat{O} = \sum_\Omega [\hat{O}]_\Omega$. The merit of using the eigenvalue decomposition is that the time evolution of the operators is explicitly given by

$$\hat{O}(t) \equiv e^{\mathcal{L}t}\hat{O} = \sum_\Omega [\hat{O}]_\Omega e^{\Omega t}. \tag{6}$$

In the calculus inside trace of operator products below, the Ω-component $[\hat{O}]_\Omega$ also works as an operator (matrix) in the same manner as the original operator $\hat{O}$. Accordingly, $[[\hat{A}]_{\Omega_1}\hat{B}]_{\Omega_2}$ is understood as the Ω_2 component of a matrix product $[\hat{A}]_{\Omega_1}\hat{B}$.

2. Average filtered-field intensity

Now, we apply the eigenvalue decomposition technique to the filtered-field intensity, $\langle \hat{E}_F^+(t_j)\hat{E}_F^-(t_j)\rangle = \mathrm{Tr}[\hat{E}_F^+(t_j)\hat{E}_F^-(t_j)\hat{\rho}_{SS}]$ in Eq. (3), whereas the system is assumed to be in the steady state $\hat{\rho}(t_j) = \hat{\rho}_{SS}$. Inserting Eq. (2), we have

$$\begin{aligned}
&\langle \hat{E}_F^+(t_j)\hat{E}_F^-(t_j)\rangle \\
&= \int_0^\infty \int_0^\infty d\tau_1 d\tau_2 \; f^*(\tau_1)f(\tau_2) \\
&\quad \times \mathrm{Tr}[\hat{E}^+(t_j - \tau_1)\hat{E}^-(t_j - \tau_2)\hat{\rho}_{SS}] \\
&= \iint_{\tau_2 > \tau_1 > 0} d\tau_1 d\tau_2 \; f^*(\tau_1)f(\tau_2)\mathrm{Tr}[\hat{E}^+ e^{\mathcal{L}\tau_{21}}(\hat{E}^-\hat{\rho}_{SS})] \\
&\quad + \iint_{\tau_1 > \tau_2 > 0} d\tau_1 d\tau_2 \; f^*(\tau_1)f(\tau_2)\mathrm{Tr}[\hat{E}^- e^{\mathcal{L}\tau_{12}}(\hat{\rho}_{SS}\hat{E}^+)],
\end{aligned} \tag{7}$$

with $\tau_{ij} \equiv \tau_i - \tau_j$. Applying Eq. (6), the filtered-field intensity is expressed in the form

$$\langle \hat{E}_F^+(t_j)\hat{E}_F^-(t_j)\rangle = \sum_\Omega s(\Omega)q(\Omega) + s^*(\Omega)q^*(\Omega), \tag{8}$$

where we noticed that the first and second terms in the right-hand side of Eq. (7) are the conjugate pairs. The coefficients are given by

$$s(\Omega) = \iint_{\tau_2 > \tau_1 > 0} d\tau_1 d\tau_2 \; f^*(\tau_1)f(\tau_2)e^{\Omega\tau_{21}}, \tag{9}$$

$$q(\Omega) = \mathrm{Tr}(\hat{E}^+[\hat{E}^-\hat{\rho}_{SS}]_\Omega). \tag{10}$$

This is the general form of the superoperator eigenvalue decomposition for the filtered-field intensity. If the filter bandwidth λ is set small, the intensity $\langle \hat{E}_F^+(t_j)\hat{E}_F^-(t_j)\rangle$ as a function of the central frequency ω_F is the emission spectrum. This eigenvalue decomposition method was previously applied to the calculation of the Mössbauer spectra [23] as a first-order correlation function. The method shown here is essentially the same as that shown in the paper. However, we will now apply this method to the second-order correlation function.

3. Average filtered-field intensity correlation

Next, we compute the second-order correlation function at zero delay assuming the steady state:

$$\begin{aligned}
&\langle \mathcal{T}_+\mathcal{T}_- \hat{E}_F^+(t_1)\hat{E}_F^+(t_2)\hat{E}_F^-(t_2)\hat{E}_F^-(t_1)\rangle|_{t_1=t_2} \\
&= 2^2 \iiiint_{\substack{\tau_1 > \tau_2 > 0 \\ \tau_4 > \tau_3 > 0}} d\tau^4 f^*(\tau_1)f^*(\tau_2)f(\tau_3)f(\tau_4) \\
&\quad \times \mathrm{Tr}[\hat{E}^+(-\tau_1)\hat{E}^+(-\tau_2)\hat{E}^-(-\tau_3)\hat{E}^-(-\tau_4)\hat{\rho}_{SS}],
\end{aligned} \tag{11}$$

where $d\tau^4 \equiv d\tau_1 d\tau_2 d\tau_3 d\tau_4$. The region of the fourfold integration is divided into six regions with different time orderings: (i) $\tau_2 < \tau_3 < \tau_4 < \tau_1$, (ii) $\tau_2 < \tau_3 < \tau_1 < \tau_4$, (iii) $\tau_2 < \tau_1 < \tau_3 < \tau_4$, (iv) $\tau_3 < \tau_2 < \tau_1 < \tau_4$, (v) $\tau_3 < \tau_2 < \tau_4 < \tau_1$, and (vi) $\tau_3 < \tau_4 < \tau_2 < \tau_1$. Since the contributions from (i) and (iv), (ii) and (v), and (iii) and (vi) are complex conjugate pairs, respectively, we have only to compute the integration over (i), (ii), and (iii).

The second-order correlation function in Eq. (11), $\mathrm{Tr}[\hat{E}^+(-\tau_1)\hat{E}^+(-\tau_2)\hat{E}^-(-\tau_3)\hat{E}^-(-\tau_4)\hat{\rho}_{SS}]$, is expressed by using the quantum regression theorem and the superoperator eigenvalue decomposition, as

$$\begin{aligned}&\mathrm{Tr}(\hat{E}^+e^{\mathcal{L}\tau_{32}}\{\hat{E}^-e^{\mathcal{L}\tau_{43}}[\hat{E}^-e^{\mathcal{L}\tau_{14}}(\hat{\rho}_{SS}\hat{E}^+)]\})\\&=\sum_{\Omega_1,\Omega_2,\Omega_3}\exp(\Omega_1\tau_{14}+\Omega_2\tau_{43}+\Omega_3\tau_{32})\\&\quad\times\mathrm{Tr}(\hat{E}^+\{\hat{E}^-[\hat{E}^-(\hat{\rho}_{SS}\hat{E}^+)_{\Omega_1}]_{\Omega_2}\}_{\Omega_3})\end{aligned}\tag{12}$$

for (i) $\tau_2<\tau_3<\tau_4<\tau_1$. Similarly, it is

$$\begin{aligned}&\sum_{\Omega_1,\Omega_2,\Omega_3}\exp(\Omega_1\tau_{41}+\Omega_2\tau_{13}+\Omega_3\tau_{32})\\&\quad\times\mathrm{Tr}(\hat{E}^+\{\hat{E}^-[(\hat{E}^-\hat{\rho}_{SS})_{\Omega_1}\hat{E}^+]_{\Omega_2}\}_{\Omega_3})\end{aligned}\tag{13}$$

for (ii) $\tau_2<\tau_3<\tau_1<\tau_4$, and

$$\begin{aligned}&\sum_{\Omega_1,\Omega_2,\Omega_3}\exp(\Omega_1\tau_{43}+\Omega_2\tau_{31}+\Omega_3\tau_{12})\\&\quad\times\mathrm{Tr}(\hat{E}^+\{[\hat{E}^-(\hat{E}^-\hat{\rho}_{SS})_{\Omega_1}]_{\Omega_2}\hat{E}^+\}_{\Omega_3})\end{aligned}\tag{14}$$

for (iii) $\tau_2<\tau_1<\tau_3<\tau_4$. By inserting Eqs. (12)–(14) into Eq. (11), we obtain a general expression:

$$\begin{aligned}&\langle\mathcal{T}_+\mathcal{T}_-\hat{E}_F^+(t_1)\hat{E}_F^+(t_2)\hat{E}_F^-(t_2)\hat{E}_F^-(t_1)\rangle|_{t_1=t_2}\\&=2\mathrm{Re}\sum_{k=\mathrm{i}}^{\mathrm{iii}}\sum_{\Omega_1,\Omega_2,\Omega_3}Z_k(\Omega_1,\Omega_2,\Omega_3)\Theta_k(\Omega_1,\Omega_2,\Omega_3),\end{aligned}\tag{15}$$

where

$$\begin{aligned}Z_{\mathrm{i}}&=2^2\iiiint_{(\mathrm{i})}d\tau^4f^*(\tau_1)f^*(\tau_2)f(\tau_3)f(\tau_4)\\&\quad\times\exp(\Omega_1\tau_{14}+\Omega_2\tau_{43}+\Omega_3\tau_{32}),\end{aligned}\tag{16}$$

$$\begin{aligned}Z_{\mathrm{ii}}&=2^2\iiiint_{(\mathrm{ii})}d\tau^4f^*(\tau_1)f^*(\tau_2)f(\tau_3)f(\tau_4)\\&\quad\times\exp(\Omega_1\tau_{41}+\Omega_2\tau_{13}+\Omega_3\tau_{32}),\end{aligned}\tag{17}$$

$$\begin{aligned}Z_{\mathrm{iii}}&=2^2\iiiint_{(\mathrm{iii})}d\tau^4f^*(\tau_1)f^*(\tau_2)f(\tau_3)f(\tau_4)\\&\quad\times\exp(\Omega_1\tau_{43}+\Omega_2\tau_{31}+\Omega_3\tau_{12}),\end{aligned}\tag{18}$$

and

$$\Theta_{\mathrm{i}}=\mathrm{Tr}(\hat{E}^+\{\hat{E}^-[\hat{E}^-(\hat{\rho}_{SS}\hat{E}^+)_{\Omega_1}]_{\Omega_2}\}_{\Omega_3}),\tag{19}$$

$$\Theta_{\mathrm{ii}}=\mathrm{Tr}(\hat{E}^+\{\hat{E}^-[(\hat{E}^-\hat{\rho}_{SS})_{\Omega_1}]_{\Omega_2}\}_{\Omega_3}),\tag{20}$$

$$\Theta_{\mathrm{iii}}=\mathrm{Tr}(\hat{E}^+\{\hat{E}^-[(\hat{E}^-\hat{\rho}_{SS})_{\Omega_1}\hat{E}^+]_{\Omega_2}\hat{E}^+\}_{\Omega_3}).\tag{21}$$

With the general decomposed expression, the effect of the spectral filtering on the second-order correlation function enters only through $Z_k(\Omega_1,\Omega_2,\Omega_3)$ and $s(\Omega)$. Therefore, they can be regarded as response functions of the system in which the filter response is convolved.

We should mention here the case of short correlation time τ_c filters [τ_c is defined through $f(\tau\gg\tau_c)=0$], which should correspond to an unfiltered case. If τ_c is much shorter than the time scale of system dynamics, we can put $\exp(\Omega_i\tau_j)=1$ for Z_k in Eqs. (16)–(18) and for s in Eq. (9). In this case ($\tau_c\to0$), s and Z_k for $k=$ i–iii are independent on Ω, Ω_1,Ω_2, and Ω_3. Then, by using $\sum_{\Omega_1,\Omega_2,\Omega_3}\Theta_k=\langle\hat{E}^+\hat{E}^+\hat{E}^-\hat{E}^-\rangle$, $\sum_\Omega q(\Omega)=\langle\hat{E}^+\hat{E}^-\rangle$, we safely find that the expression for the normalized correlation function is reduced to be that of the unfiltered field:

$$g_F^{(2)}(0)=\frac{\langle\hat{E}^+\hat{E}^+\hat{E}^-\hat{E}^-\rangle}{\langle\hat{E}^+\hat{E}^-\rangle^2}.\tag{22}$$

4. s and Z_k for Lorentzian, Gaussian, and rectangular filters

As the typical examples, the above general expression is applied to three types of filters—Lorentzian, Gaussian, and rectangular filters—to obtain the explicit analytic forms for s and Z_k here. In the calculation, we assume for simplicity that the time delay of the filter response, τ_d in Fig. 2(a), is much larger than the correlation time, τ_c, and in addition the system is assumed to be in the steady state. Under this assumption, we will change the time variables from τ to $\tau+\tau_d$ and approximately change the lower limit of the time integration from zero to $-\tau_d\approx-\infty$. With this change, the range of the integration for $s(\Omega)$ is replaced by $-\infty<\tau_1<\tau_2<\infty$ in Eq. (9). Similarly, for Z_k in Eqs. (16)–(18), the time range of the integration is replaced by $-\infty<\tau_j<\infty$ while the ordering among τ_1, τ_2, τ_3, and τ_4 is unchanged.

The Lorentzian filter is the simplest example to perform the time integration to give s ($=s^L$) and Z_k ($=Z_k^L$), since the correlation function of Lorentzian filter $f(\tau)=f_L(\tau)$ is an exponential [21]:

$$f_L(\tau)=\lambda\theta(\tau)\exp[(-\lambda-i\omega_F)\tau],\tag{23}$$

where $\theta(x)$ is the Heaviside step function. Inserting this and after straightforward integrations, we find that they are given by simple polynomial fractions:

$$s^L(\Omega)=\frac{\lambda/2}{i\omega_F+\lambda-\Omega},\tag{24}$$

$$Z_{\mathrm{i}}^L=\frac{\lambda}{\lambda-i\omega_F-\Omega_1}\frac{\lambda}{2\lambda-\Omega_2}\frac{\lambda}{3\lambda+i\omega_F-\Omega_3},\tag{25}$$

$$Z_{\mathrm{ii}}^L=\frac{\lambda}{\lambda+i\omega_F-\Omega_1}\frac{\lambda}{2\lambda-\Omega_2}\frac{\lambda}{3\lambda+i\omega_F-\Omega_3},\tag{26}$$

$$Z_{\mathrm{iii}}^L=\frac{\lambda}{\lambda+i\omega_F-\Omega_1}\frac{\lambda}{2\lambda+i2\omega_F-\Omega_2}\frac{\lambda}{3\lambda+i\omega_F-\Omega_3}.\tag{27}$$

For Lorentzian filters, the time integration for correlation functions gives the products of the transfer function, and therefore analytic time integration up to the arbitrarily high orders is possible. For simplicity, the photon statistics of filtered fields has been studied only for Lorentzian filters [15,21]. However, as shown in the next section, when the time scale of the system dynamics is comparable to τ_c, which we sometimes face in state-of-the-art quantum emitters, the best choice of the filter type is essential. Therefore, the photon statistics of the field filtered by other types of filters should be necessary. Here we just show the results for Gaussian and rectangular filters (but the method can be applied to arbitrary filter function).

For Gaussian filters, the correlation functions, $f(\tau)$ [$=f_G(\tau)$] in the time domain and $F(\omega)$ [$=F_G(\omega)$] in the

TABLE I. Coefficients for Z_k^G of Gaussian filters, Eq. (31).

k	A_k	B_k	C_k
i	$\frac{\Omega_1-\Omega_2+\Omega_3}{2\lambda}$	$\frac{-2i\omega_F-\Omega_1+\Omega_3}{2\lambda}$	$\frac{-\Omega_2}{2\lambda}$
ii	$\frac{-2i\omega_F+\Omega_1-\Omega_2+\Omega_3}{2\lambda}$	$\frac{-\Omega_1+\Omega_3}{2\lambda}$	$\frac{-\Omega_2}{2\lambda}$
iii	$\frac{\Omega_1-\Omega_2+\Omega_3}{2\lambda}$	$\frac{-\Omega_1+\Omega_3}{2\lambda}$	$\frac{2i\omega_F-\Omega_2}{2\lambda}$

TABLE II. Coefficients for Z_k^r of rectangular filters, Eq. (35).

k	α_k	β_k	γ_k
i	$\frac{-\omega_F-i\Omega_3}{\lambda}+i0$	$\frac{-i\Omega_2}{\lambda}+i0$	$\frac{\omega_F+\lambda-i\Omega_1}{\lambda}+i0$
ii	$\frac{-\omega_F-i\Omega_3}{\lambda}+i0$	$\frac{-i\Omega_2}{\lambda}+i0$	$\frac{-\omega_F+\lambda-i\Omega_1}{\lambda}+i0$
iii	$\frac{-\omega_F-i\Omega_3}{\lambda}+i0$	$\frac{-2\omega_F-i\Omega_2}{\lambda}+i0$	$\frac{-\omega_F+\lambda-i\Omega_1}{\lambda}+i0$

frequency domain are

$$f_G(\tau)=\frac{\lambda}{\sqrt{\pi}}\exp[-(\lambda\tau)^2-i\omega_F\tau], \tag{28}$$

$$F_G(\omega)=\frac{1}{2\pi}\exp\left[-\left(\frac{\omega-\omega_F}{2\lambda}\right)^2\right], \tag{29}$$

where the Fourier transform is defined by $F(\omega)\equiv(2\pi)^{-1}\int f(\tau)\exp(i\omega\tau)d\tau$. For this filter, $s(\Omega)$ $[=s^G(\Omega)]$ is given by

$$s^G(\Omega)=\tfrac{1}{2}\exp[y(\Omega)^2]\{1+\mathrm{erf}[y(\Omega)]\}, \tag{30}$$

where $y(\Omega)\equiv(\Omega-i\omega_F)/(\sqrt{2}\lambda)$ and $\mathrm{erf}(x)$ is the Gauss error function. For the second-order correlation function, we obtained an analytic expression for Z_k $(=Z_k^G)$:

$$Z_k^G=\frac{1}{\sqrt{\pi}}e^{A_k^2+B_k^2+C_k^2}\int_0^\infty e^{-(z-A_k)^2}[1-\mathrm{erf}(z+C_k)] \times[\mathrm{erf}(z+B_k)-\mathrm{erf}(-z+B_k)]dz, \tag{31}$$

the coefficients of which—A_k, B_k, and C_k—are given in Table I.

For rectangular filters, filter correlation functions $f(\tau)$ $[=f_r(\tau)]$ and $F(\omega)$ $[=F_r(\omega)]$ are given by

$$f_r(\tau)=\exp(-i\omega_F\tau)\frac{\sin(\lambda\tau)}{\pi\tau}, \tag{32}$$

$$F_r(\omega)=\frac{1}{2\pi}\theta(\lambda-|\omega-\omega_F|). \tag{33}$$

For this filter, $s(\Omega)$ $[=s^r(\Omega)]$ is found to be

$$s^r(\Omega)=\frac{1}{2\pi i}\ln\left(\frac{\omega_F+\lambda+i\Omega-i0}{\omega_F-\lambda+i\Omega-i0}\right), \tag{34}$$

where the infinitesimally small positive number, zero, is introduced for the analytic continuation of the logarithmic function [which is essential in case $\mathrm{Re}(\Omega)=0$]. The analytic expression for Z_k $(=Z_k^r)$ is also found by inserting Eq. (32) into Eqs. (16)–(18) and performing the integration

$$Z_k^r=\frac{i}{2\pi^3}\{[\phi(\alpha_k^+,\beta_k^+;2)+\phi(\alpha_k^-,\beta_k^-;-2)] \times[\ln(2-\gamma_k)-\ln(-\gamma_k)] -\Phi(\alpha_k^+,\beta_k^+,\gamma_k;2)+\Phi(\alpha_k^-,\beta_k^-,\gamma_k-2;-2)\}, \tag{35}$$

where $\alpha_k^\pm\equiv\alpha_k\pm1$; $\beta_k^\pm\equiv\beta_k\pm2$; and the coefficients α_k, β_k, and γ_k are given in Table II. The functions ϕ and Φ are defined with an analytically continued function of the nth-order polylogarithm, $\mathrm{Li}_n(z)=\sum_{m=1}^\infty z^m/m^2$, by

$$\phi(a,b;z)\equiv-\ln(z-b)\ln(-a) +\ln(z-a)\ln\left(\frac{z-b}{a-b}\right)+\mathrm{Li}_2\left(\frac{z-a}{b-a}\right), \tag{36}$$

$$\Phi(a,b,c;z)\equiv\int_0^z\frac{\phi(a,b;z)}{z-c}dz. \tag{37}$$

In the evaluation of Z_k^r, we have carefully performed the multiple complex integrations since the contours cross branch cuts of the logarithmic functions.

To summarize this section, a simple calculation method for photon statistics of the filtered field, based on superoperator eigenvalue decomposition technique, was proposed and analytic expressions for s and Z_k are obtained for the three types of filters: Lorentzian, Gaussian, and rectangular filters (as typical examples). For other types of filters, it will also be possible to find analytic expressions, although we will not go into further details here. Validity of our method is confirmed numerically by the perfect agreements with the other method [15] for the case of Lorentzian filters, as shown in Sec. III.

III. APPLICATION TO QUANTUM DOT SINGLE-PHOTON EMITTERS

Here, we take QDs as an example of efficient SP emitters and apply the proposed eigenvalue decomposition method to a simulation of the photon statistics of the emission field filtered by Lorentzian, Gaussian, and rectangular filters.

A. QD SP emitters under incoherent pumping

The model of the QD emitter system is the same as that used in our previous paper [14,26,27]. We consider the QD emitter states consisting of the electron-hole carriers as shown in Fig. 3(a). Among 16 carrier configurations occupying the lowest-energy levels, six charge-neutral configurations are taken into account: an empty state $|G\rangle$, two bright exciton (BX) states $|\mathrm{BX1}\rangle=\hat{e}_\uparrow^\dagger\hat{h}_\downarrow^\dagger|G\rangle$ and $|\mathrm{BX2}\rangle=\hat{e}_\downarrow^\dagger\hat{h}_\uparrow^\dagger|G\rangle$, two dark exciton (DX) states $|\mathrm{DX1}\rangle=\hat{e}_\uparrow^\dagger\hat{h}_\uparrow^\dagger|G\rangle$ and $|\mathrm{DX2}\rangle=\hat{e}_\downarrow^\dagger\hat{h}_\downarrow^\dagger|G\rangle$, and a biexciton state $|\mathrm{XX}\rangle=\hat{e}_\uparrow^\dagger\hat{e}_\downarrow^\dagger\hat{h}_\uparrow^\dagger\hat{h}_\downarrow^\dagger|G\rangle$, where $\hat{e}_\sigma$ and $\hat{h}_\sigma$ ($\hat{e}_\sigma^\dagger$ and $\hat{h}_\sigma^\dagger$) are annihilation (creation) operators of electrons and holes with spin $\sigma=\uparrow,\downarrow$ in their respective lowest-energy levels of the QD. The Hamiltonian of the QD emitter is

$$\hat{H}=\omega_X\hat{N}_{\mathrm{tot}}-\chi|\mathrm{XX}\rangle\langle\mathrm{XX}|, \tag{38}$$

where $\hat{N}_{\mathrm{tot}}=\sum_{\sigma=\uparrow,\downarrow}(\hat{e}_\sigma^\dagger\hat{e}_\sigma+\hat{h}_\sigma^\dagger\hat{h}_\sigma)/2$ is the number of excitons, $\chi(=\omega_X-\omega_{XX})$ is the biexciton binding energy, and the fine-structure splitting between the exciton states is neglected. The following incoherent decay processes are considered as

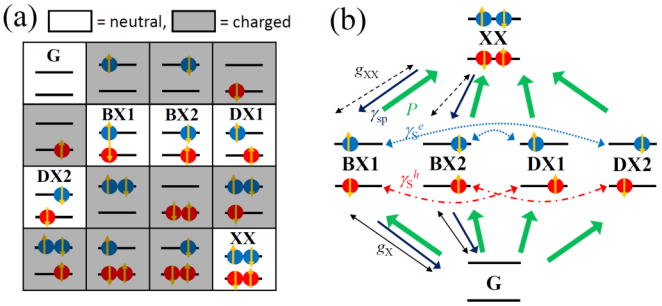

FIG. 3. (Color online) A neutral QD model [14,26,27]. (a) Among 16 electronic states at the QD ground levels, six neutral states with up to two excitons (G, BX1, BX2, DX1, DX2, and XX) are taken into account. (b) Incoherent pump (P) and decay processes (γ_{sp}, γ_S^e, γ_S^h).

shown in Fig. 3(b): the decay of the injected electron-hole pairs is dominated by the spontaneous emission (the rate γ_{sp}) [28], the excitons suffer dephasing (with the rate $\Gamma_{\rm ph}$), and the spin flip of electrons and holes (with the rates γ_S^e and γ_S^h) results in the transitions between dark and bright exciton states with a rate γ_S ($=\gamma_S^e+\gamma_S^h$). The above-band-gap laser excitation followed by the fast carrier relaxation to the QD ground states or the carrier current injection are modeled by an incoherent pumping rate, P [14].

In this neutral QD, it was shown that XX emission at $\omega=\omega_X-\chi$ is enhanced by incoherent XX excitation via DX states, and can strongly degrade the purity of SP emissions, especially in the case when the spin-flip process is slower than the spontaneous emission ($\gamma_S<\gamma_{sp}$) [14]. Therefore, if the exciton emission at $\omega=\omega_X$ is applied to a SP source, the XX emission must be effectively cut by using a spectral filter. Here, for the calculation of the emission properties, we define the emission field operator for the BX recombination by $\hat{E}^-\equiv\sum_\sigma \hat{e}_\sigma \hat{h}_{-\sigma}=(\hat{E}^+)^\dagger$, and the central frequency of the filter ω_F is set as $\omega_F=\omega_X$.

In Fig. 4(a), the emission spectrum is shown for a situation ($\chi=2$ meV, $\Gamma_{\rm ph}=20$ μeV, $1/\gamma_S=10$ ns, $1/\gamma_{sp}$=1 ns). In the same figure, the filter functions in the frequency domain $|F(\omega)|^2$ are also shown for Lorentzian, Gaussian, and rectangular filters with the bandwidth $\lambda=300$ μeV. In the frequency domain, the Lorentzian filter has a long tail, Gaussian filter has a shorter tail, and rectangular filter has an ideally sharp cut. Therefore, from the emission spectrum, the rectangular filter (with a bandwidth less than $\chi=2$ meV) may be expected to be the most effective filter, but we see in the following that the real situation is not so simple.

In Fig. 4(b), we show the $g^{(2)}(0)$ obtained for the emission spectrally filtered by the three types of filters as a function of the bandwidth λ. As expected, the $g^{(2)}(0)$ is reduced if the bandwidth is chosen as $\lambda<\chi$ for all filters. On the other hand, if the bandwidth is chosen too small, $g^{(2)}(0)$ increases as λ decreases due to the increased time uncertainty ($\Delta t=\tau_c=1/\lambda$ in Fig. 2) as mentioned above and in previous literature [21]. Therefore, by considering the two opposing effects, spectral suppression of the unwanted detection of XX emissions and increasing time uncertainty (decreasing time resolution) for too narrow filters, the existence of the optimal filter bandwidth $\lambda_{\rm opt}$ is expected. As predicted from the above argument, we found the $g^{(2)}(0)$ shows the minima (=0.0027 for Lorentzian, 0.0025 for Gaussian, and 0.0048 for rectangular filters) in Fig. 4(b) ($\Gamma_{\rm ph}<\lambda_{\rm opt}<\chi$ where $\Gamma_{\rm ph}$ gives the exciton linewidth). Here, we note that our results for the Lorentzian filter perfectly agree with those obtained by using the other method [15], numerically showing the validity of our method.

The above findings, e.g., the existence of an optimal filter bandwidth at $\Gamma_{\rm ph}<\lambda_{\rm opt}<\chi$, seem to be trivial. However, the following findings are rather counterintuitive.

(i) The rectangular filter has the largest minimum value of $g^{(2)}(0)$ among the three filters although the rectangular filter ideally cuts the XX emission in the frequency domain.

(ii) The optimal filter bandwidth $\lambda_{\rm opt}$ is much larger than the emission linewidth $\sim\Gamma_{\rm ph}$. (i) also applies to a wide range of the XX binding energy (0.5 meV $<\chi<$ 8 meV) as seen in Fig. 4(c), where the minima of $g^{(2)}(0)$ as a function of χ are shown for the three filters.

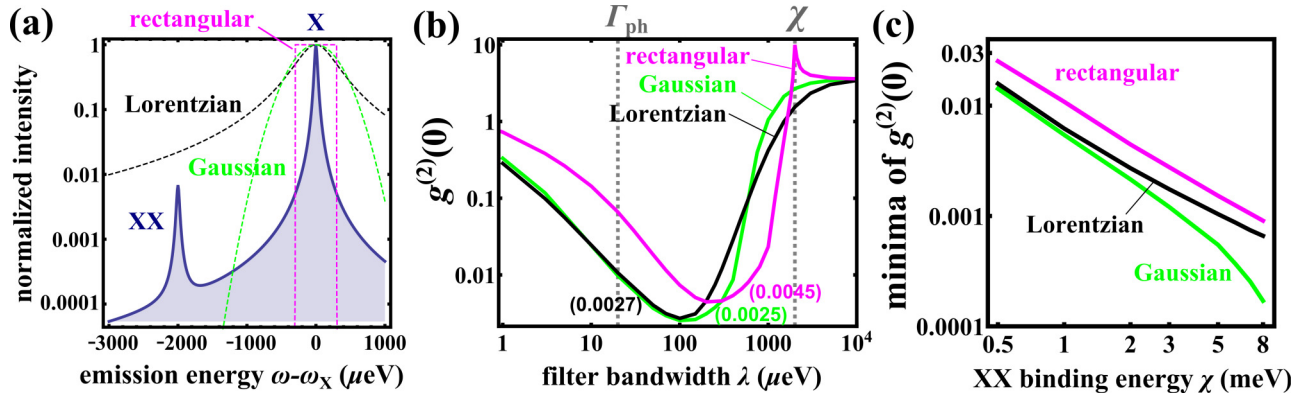

FIG. 4. (Color online) (a) The emission spectrum of a QD SP emitter (solid) for XX binding energy $\chi=2000$ μeV is shown with the normalized filter functions $|F(\omega)|^2$ (dashed) for Lorentzian (black), Gaussian (green), and rectangular (magenta) filters with $\lambda=300$ μeV. (b, c) $g^{(2)}(0)$ of the QD emission after spectral filtering by the three types of filters, Lorentzian (black), Gaussian (green), and rectangular (magenta). (b) Filter bandwidth (λ) dependence for XX binding energy $\chi=2000$ μeV. (c) The χ dependence of $g^{(2)}(0)$ at the optimal filter bandwidth $\lambda_{\rm opt}$ [$\approx$ 100 μeV for the Lorentzian filter in (b); $g^{(2)}(0)$ at $\lambda_{\rm opt}$ are also indicated in (b)]. We set (γ_{sp}, $\Gamma_{\rm ph}$) = (0.67,20) μeV, small pump rate P in the linear regime [14], and the spin-flip time $\tau_S\equiv\gamma_S=10$ ns for all figures.

Figure 4(c) shows that the Gaussian filter will be the best filter to purify the SP emission from this neutral QD system (after the optimization of the bandwidth). (i) can be understood as the difference of the filter correlation function in the time domain, $f(\tau)$. The $f(\tau)[= f_r(\tau)]$ in Eq. (32) is the sinc function with the slow power-law decay at large τ, different from the fast exponential decay for the other two filters. Therefore, the increase in the time uncertainty matters significantly if a rectangular filter is used. In the case of the Gaussian filter, because the correlation function is Gaussian also in the time domain, the long-time tail is strongly suppressed compared with the rectangular filter. Therefore, the lower value of $g^{(2)}(0)$ in Fig. 4(c) with the Gaussian filter is reasonable.

Here we briefly comment on the effect of the dephasing and broadening, since they are the key parameters for solid-state QD emitters. According to the same numerical simulation for a larger dephasing rate, $\Gamma_{\rm ph} = 100\ \mu$eV, we found that the results corresponding to Figs. 4(b) and 4(c) are qualitatively the same whereas the $g^{(2)}(0)$ value itself is increased due to the increased broadening (not shown). Spectral broadening is also caused by coupling the QDs to a small cavity due to the Purcell effect. In this case, a cavity plays two roles: One is the spectral broadening increasing $g^{(2)}(0)$, and the other is the cavity effect as a (Lorentzian) spectral filter with the bandwidth equal to the cavity loss rate. Because of the latter effect, there is an optimal cavity loss [14], being similar to Fig. 4(b).

B. SP emitters under coherent pumping

Our next example to study the filtering effect is a resonantly driven SP emitter. The resonantly scattered light by an emitter exhibits the Mollow triplet emission spectrum [29], which can be applied to an indistinguishable SP source [3,11,12,21], since the resonant excitation prevents emitters from suffering spectral diffusion and dark exciton effects, and by reducing dephasing processes.

The physics of the SP emission from the scattered light is illustrated in Fig. 5(a). In the presence of a coherent laser field (frequency ω_L) in resonance with the emitter ($\omega_X = \omega_L \equiv \omega_0$), the scattered light is known to exhibit the Mollow triplet [25] [Fig. 5(b)] with a central (C) peak and two side peaks (L, U). The three peaks in the fluorescence spectrum correspond to the transitions (arrows) between the dressed states indicated by C (dash-dotted), L (dashed), and U (solid), respectively in Fig. 5(a). From the illustration, the side peak (say the upper, U) is successively followed by emissions of the other side (L) or central (C) peaks. Therefore, successive two-photon emission within the same side peak is strongly suppressed if the splitting between the dressed states is larger than the linewidth ($2\Omega_{\rm R} \gg \gamma_{sp}$ if the linewidth is limited by the emitter lifetime). This scheme to produce highly efficient and distinguishable single photons has been studied in recent years with QD emitters [3,11,12,21], in which the spectral filtering of a side peak emission (say $\omega = \omega_0 + 2\Omega_{\rm R}$) is essential. In this scheme, the major cause of the contamination noise on the SP purity is the other two emission peaks ($\omega = \omega_0,\ \omega_0 - 2\Omega_{\rm R}$) and the excitation laser itself ($\omega = \omega_0$). The main physics can be described by a resonantly driven two-level system (TLS):

$$\frac{d}{dt}\hat{\rho} = i[\hat{\rho}, \hat{H}] + \gamma_{sp}\mathcal{L}_{\hat{\sigma}^-}\hat{\rho} + (\Gamma_{\rm ph}/2)\mathcal{L}_{\hat{\sigma}_z}\hat{\rho}, \tag{39}$$

where $\hat{H} = \Omega_{\rm R}\hat{\sigma}^+ + \Omega_{\rm R}^*\hat{\sigma}^-$ in the rotating frame, and γ_{sp} and $\Gamma_{\rm ph}$ are the spontaneous emission and dephasing rates.

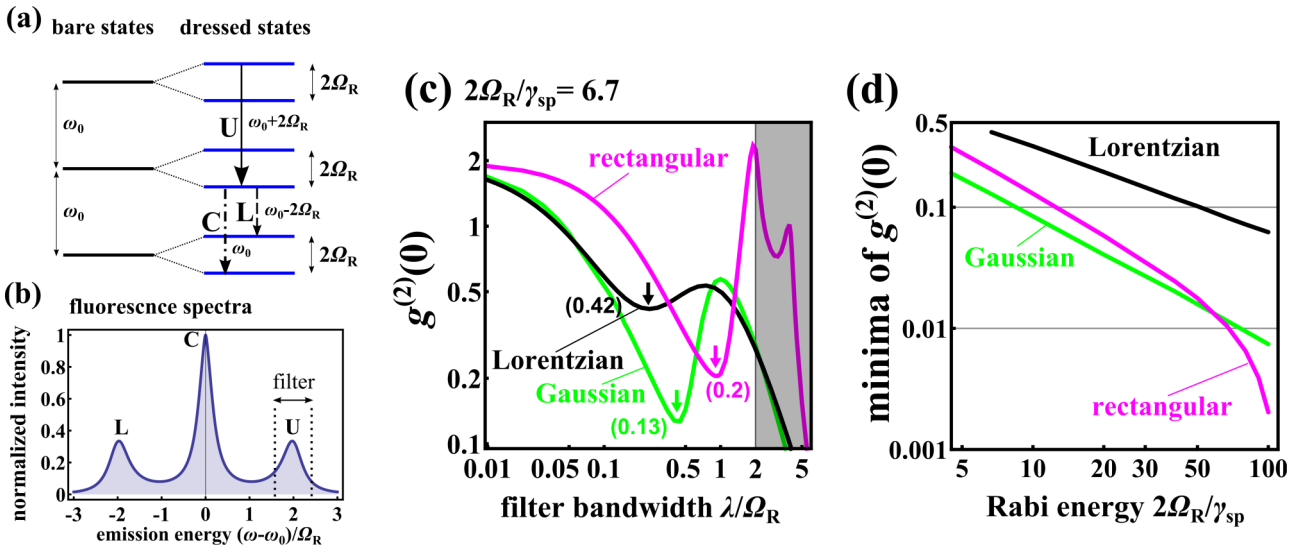

FIG. 5. (Color online) Illustration of the single-photon emission from coherently driven emitters (the Rabi frequency $\Omega_{\rm R}$ and $\omega_0 \equiv \omega_L = \omega_X$, laser frequency ω_L, and the emitter transition frequency ω_X). (a) The bare and dressed energy levels with the radiative transitions marked by arrows corresponding to the emission peaks in (b), and (b) the fluorescence spectrum showing Mollow triplets, a central peak (C) at $\omega = \omega_0$, and upper (U) and lower (L) side peaks. The $g^{(2)}(0)$ of the upper side peak emission (U) spectrally selected by three types of filters with $\omega_F = \omega_0 + 2\Omega_{\rm R}$, Lorentzian (black), Gaussian (green), and rectangular (magenta). (c) $g^{(2)}(0)$ as a function of the normalized filter bandwidth $\lambda/\Omega_{\rm R}$. (d) $g^{(2)}(0)$ minimized in the range $0 < \lambda < 2\Omega_{\rm R}$ as a function of the normalized Rabi energy $\Omega_{\rm R}/\gamma_{\rm sp}$ (the values inside brackets and arrows indicate the minima in (c); the upper limit of the range is set in order to avoid the detection of the driving laser light in the shaded area, $\lambda > 2\Omega_{\rm R}$). We set the spontaneous emission $\gamma_{sp} = 0.3\Omega_{\rm R}$ and dephasing rate $\Gamma_{\rm ph} = 0$ for (b) and (c), and the dephasing rate $\Gamma_{\rm ph} = 0$ for all figures.

First we set the dephasing rate $\Gamma_{\rm ph} = 0$ according to the experimental reports showing lifetime limited linewidth [12]. For the calculation of the emission properties, we define the emission field operator by $\hat{E}^{\pm} \equiv \hat{\sigma}^{\pm}$, and the central frequency of the filter ω_F is set as $\omega_F = \omega_0 + 2\Omega_{\rm R}$.

Figure 5(c), shows the simulated $g^{(2)}(0)$ of the upper side peak emissions spectrally filtered by the three types of filters—Lorentzian (black), Gaussian (green), and rectangular (magenta) filters. The $g^{(2)}(0)$ is plotted as a function of the filter bandwidth λ, which shows a minimum in the regime $0 < \lambda < 2\Omega_{\rm R}$ reflecting the physics of SP generation mentioned above. If $\lambda < 2\Omega_{\rm R}$, $g^{(2)}(0)$ decreases as λ decreases since the spectral selection for the side peak becomes effective. On the other hand, for λ much less than the spontaneous emission rate γ_{sp} or the linewidth [$\gamma_{sp} = 0.3\Omega_{\rm R}$ in Fig. 5(c)], $g^{(2)}(0)$ increases as λ decreases due to the degraded time resolution. The $g^{(2)}(0)$ at the minima depends on the types of the spectral filters, being similar to Fig. 4(b), the result for an incoherently pumped QD. In this case, however, the Gaussian filter gives the smallest $g^{(2)}(0)$, i.e., the most pure SP emission, and the Lorentzian filter gives the worst purity for $\gamma_{sp} = 0.3\Omega_{\rm R}$ ($2\Omega_{\rm R}/\gamma_{sp} = 6.7$) in Fig. 5(c). Here, we again note that our results for the Lorentzian filter perfectly agree with those obtained by using the other method [15], numerically showing the validity of our method.

In Fig. 5(d), the $g^{(2)}(0)$ at the minima is shown as a function of the ratio between the Rabi frequency over the linewidth, $2\Omega_{\rm R}/\gamma_{sp}$. It is clearly found that $g^{(2)}(0)$ at the minima decreases (i.e., the SP purity increases) as $2\Omega_{\rm R}/\gamma_{sp}$ increases. This is because the contamination source, i.e., the other emission peaks, C and L, becomes spectrally separated and suppressed well by the filters for larger splitting, $2\Omega_{\rm R}/\gamma_{sp}$. An interesting feature is that the Lorentzian filter gives $g^{(2)}(0)$ larger than others, i.e., the performance to obtain high SP purity is the lowest among the three types, while the rectangular filter was the worst choice in the case of incoherent excitation in Fig. 4(c). Moreover, an interesting result is that the most efficient filter type to give the highest SP purity depends on the pump parameter $2\Omega_{\rm R}/\gamma_{sp}$ in Fig. 5(d). For the Rabi splitting not too large $2\Omega_{\rm R}/\gamma_{sp} < 60$, the Gaussian filter with the smallest $g^{(2)}(0)$ is the best choice among the three. For the strong Rabi field $2\Omega_{\rm R}/\gamma_{sp} > 60$, the rectangular filter with the smallest $g^{(2)}(0)$ is the best filter type. We should note here that the latter case especially is quite different from the result of incoherent excitation in Fig. 4(c). We performed the same numerical analysis for a case including finite dephasing rate ($\Gamma_{\rm ph} = 5\gamma_{sp}$, not shown). Although the value of $g^{(2)}(0)$ is increased due to the dephasing-induced spectral broadening, we found a similar dependency of $g^{(2)}(0)$ at minima on $2\Omega_{\rm R}/\gamma_{sp}$, i.e., the rectangular filter becomes the most efficient filter for large $2\Omega_{\rm R}/(\gamma_{sp} + 2\Gamma_{\rm ph})$.

We interpret the origin of the different results between coherent and incoherent pumping as a kind of resonance phenomenon between the Rabi oscillation dynamics of TLS (with a frequency $2\Omega_{\rm R}$) and the oscillatory response [$\propto \sin(\lambda\tau)$], which will uniquely happen under coherent pumping together with the rectangular filter used. The resonance phenomenon consequently highlights the quantum correlation of the filtered field in a coherent regime $2\Omega_R/\gamma_{sp} \gg 1$ if one of the resonance conditions is satisfied on the filter bandwidth ($\lambda = \Omega_{\rm R}$, $2\Omega_{\rm R}$, and $4\Omega_{\rm R}$ as shown below). The resonance feature is not found for Gaussian or Lorentzian filters without such oscillatory components in the response function. This interpretation is mathematically explained as follows.

Here, we focus on $Z_k(\Omega_1,\Omega_2,\Omega_3)$ since the filter response is included only through it. For a TLS resonantly driven in the coherent regime $2\Omega_R/\gamma_{sp} \gg 1$, the eigenvalue Ω of $\mathcal{L}$ is approximately given by one of $(0, -\gamma_{\rm sp}/2, -3\gamma_{\rm sp}/4 \pm i2\Omega_{\rm R})$ in the rotating frame ($\omega \to \omega - \omega_0$). Therefore, up to the zeroth order in $\gamma_{\rm sp}$, $\Omega_j = i\eta_j 2\Omega_R$ where $\eta_j \in (-1,0,1)$. By rewriting Eq. (32) as $f_r(\tau_j) = (i2\pi\tau_j)^{-1}\sum_{l_j} l_j e^{i(l_j\lambda-\omega_F)\tau_j}$ where the sum is taken over $l_j = \pm 1$, the oscillatory component in the integrand, e.g., for $Z_{\rm i}$ in Eq. (16) (except for the slowly decaying component $\propto \prod_j \tau_j^{-1}$), is

$$\begin{aligned} e^{i\omega_F(\tau_1+\tau_2-\tau_3-\tau_4)} &\times e^{i\lambda(l_1\tau_1+l_2\tau_2-l_3\tau_3-l_4\tau_4)} \\ &\times e^{\Omega_1\tau_{14}+\Omega_2\tau_{43}+\Omega_3\tau_{32}} = e^{i(l_1+l_2-l_3-l_4)\lambda\tau_2} \\ &\times e^{i[l_1\lambda+(\eta_1+1)2\Omega_R]\tau_{14}} \times e^{i[(l_1-l_4)\lambda+\eta_2 2\Omega_R]\tau_{43}} \\ &\times e^{i[(l_1-l_3-l_4)\lambda+(\eta_3-1)2\Omega_R]\tau_{32}}, \end{aligned} \tag{40}$$

where $\omega_F = 2\Omega_{\rm R}$ in the rotating frame is assumed in the right-hand side. From the oscillation components, the integral becomes large if resonance conditions are satisfied, i.e., when the coefficients of $\tau_2, \tau_{14}, \tau_{43}$, and τ_{32} are vanished. By considering the case $l_1 + l_2 - l_3 - l_4 = 0$ [thus we can replace $l_1 - l_3 - l_4 \to -l_2$ in the last line in Eq. (40)], we find the exponents can be vanished when $\lambda = \Omega_{\rm R}$ and fully vanished when $\lambda = 0$, $2\Omega_{\rm R}$, and $4\Omega_{\rm R}$. Among the four conditions, we consider only the three with nonzero λ will cause large enhancement in the quantum correlation of the filtered field, since the increased time uncertainty at $\lambda = 0$ will mask the feature of quantum emissions as already discussed above. Besides, we can naively expect the resulting photon statistics is strongly dependent on λ close to the resonance conditions $\lambda \sim \Omega_{\rm R}, 2\Omega_{\rm R}$, and $4\Omega_{\rm R}$. Such a resonance feature will become clear when the decay rate γ_{sp}, neglected in Eq. (40), is small enough to fulfill $2\Omega_R/\gamma_{sp} \gg 1$. The same discussion holds for $Z_{\rm ii}$ and $Z_{\rm iii}$ as well.

In Fig. 6, we show $g^{(2)}(0)$ as a function of the filter bandwidth for a strong Rabi field $2\Omega_{\rm R}/\gamma_{sp} = 100 \gg 1$ (solid line) and for the weaker field $2\Omega_{\rm R}/\gamma_{sp} = 6.7$ [dotted line, the same as Fig. 5(c)]. By comparing the two results, as expected in the above discussion, singular behavior is found at the three resonance conditions: $\lambda \sim \Omega_{\rm R}$, $2\Omega_{\rm R}$, and $4\Omega_{\rm R}$. Two sharp peaks found at $\lambda \sim 2\Omega_{\rm R}$ and $4\Omega_{\rm R}$ indicate strong bunching effects [large $g^{(2)}(0)$] caused by the detection channel opened for cascaded emissions [e.g., for $\lambda \sim 2\Omega_{\rm R}$, the detection of the cascaded emissions U $\to$ L/C and C $\to$ C/L/U becomes possible in Fig. 5(a)]. Especially for the strong Rabi field ($2\Omega_{\rm R}/\gamma_{sp} = 100$), the bunching feature is highlighted, while on the other hand the height and sharpness of the bunching peak [the value of $g^{(2)}(0)$] are decreased as the parameter $2\Omega_{\rm R}/\gamma_{sp}$ is decreased to 6.7 (dotted line). It is reasonable to consider that a kind of constructive interference enhances the cascaded emission detection for large $2\Omega_{\rm R}/\gamma_{sp}$ if one selects $\lambda \sim 2\Omega_{\rm R}$ and $4\Omega_{\rm R}$. On the other hand, the strong dip (antibunching dip) at $\lambda \sim \Omega_{\rm R}$ is clear for $2\Omega_{\rm R}/\gamma_{sp} = 100$, while it is less clear for $2\Omega_{\rm R}/\gamma_{sp} = 6.7$. This antibunching dip is reasonably interpreted as a kind of destructive interference suppressing the

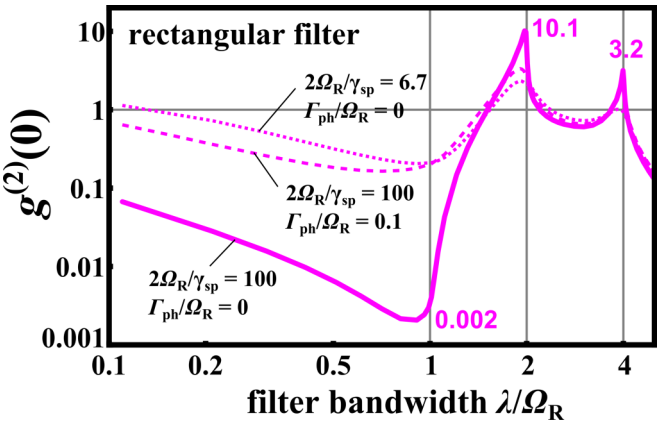

FIG. 6. (Color online) $g^{(2)}(0)$ as a function of the filter bandwidth λ/Ω_R for a rectangular filter with different decay parameters $(2\Omega_R/\gamma_{sp}, \Gamma_{ph}/\Omega_R)$: (100, 0) for the solid line, (100, 0.1) for the dashed line, and (6.7, 0) for the dotted line [same as Fig. 5(c)]. For the solid line, the $g^{(2)}(0)$ values at the dip and two peaks are indicated.

detection of the cascaded emission, which becomes effective for large $2\Omega_R/\gamma_{sp}$ if one selects $\lambda \sim \Omega_R$.

All the numerical results in Fig. 6 reasonably agree with the above-discussed resonance feature. Furthermore we can generalize the discussion to include the dephasing effect. A comparison between the solid curve and the dashed curve (with the same $2\Omega_R/\gamma_{sp} = 100$ but with finite dephasing $\Gamma_{ph} = 0.1\Omega_R$) shows that the dephasing weakens the resonance feature; the bunching at $\lambda \sim 2\Omega_R$ and $4\Omega_R$ and antibunching at $\lambda \sim \Omega_R$ are all weakened. This is because the dephasing, the additional decay channel of the coherent Rabi dynamics, increases the negative real part of Ω_j and has an effect similar to increasing γ_{sp}. To summarize, in the presence of the dephasing, we can roughly understand the results from those without dephasing by replacing γ_{sp} with $\gamma_{sp} + 2\Gamma_{ph}$.

It should be noted that the resonance phenomenon (between the quantum dynamics of the emitter system and the filter response) is a unique feature to the rectangular filter (among three filters considered in this paper), and therefore the resonance behavior at the conditions is not found in Fig. 5(c) for Lorentzian and Gaussian filters. We consider this is the reason why the strong suppression of $g^{(2)}(0)$ at the minima occurs uniquely with the rectangular filter for the case of coherent pumping at $2\Omega_R/\gamma_{sp} > 60$ in Fig. 5(d).

IV. SUMMARY

We proposed a calculation method, based on the superoperator eigenvalue decomposition technique, for photon statistics of spectrally filtered fields with various types of filters. This method can give exact results when the emission dynamics is given by quantum master equations, which can be applied to a wide variety of quantum emitters, and solvable with the eigenvalue approach (matrix diagonalization). Also, it is possible to treat a wide variety of filter functions if analytic expressions for the convolution functions, s and Z_k in Eq. (9) and Eqs. (16)–(18), respectively, are obtained.

As typical examples, focusing on three filter types—Lorentzian, Gaussian, and rectangular filters—we applied this method to QD single-photon (SP) emitters. With the simulation for two cases, under incoherent excitations and under coherent and resonant excitations, we found condition-dependent matching between filter types and emitters in order to have the highest SP purity. Especially under coherent excitations with strong Rabi field, multiple photon detection can be suppressed close to a resonance condition ($\lambda \sim \Omega_R$) with a rectangular filter.

Finally, we mention the precision of the correlation measurement to observe the filter effects in current state-of-the-art experiments. In conventional measurements, the background noise, which can be due to background emissions, dark count of photodetectors, stray light from excitation lasers, etc., has typically inhibited us from observing small values of $g^{(2)}(0)$. However, thanks to the recent development of superconducting nanowire single-photon detectors (SSPD), the dark count rate and the detection response time can be remarkably reduced. In addition, a resonant laser excitation to the excited states in a QD is shown to reduce significantly the background emission noise, by which small values of $g^{(2)}[0]$ down to 0.003 were obtained recently together with the use of SSPD [30]. In such precision experiments, the difference due to the choice of spectral filters will be detectable.

As for the SP emission from a Mollow triplet side peak, the corresponding experiments have been recently reported to show $g^{(2)}(0) < 0.1$ [31] after deconvolution of the response of avalanche photodiodes, the response of which can become faster by using SSPD. In these experiments, the stray light from the excitation laser was effectively suppressed by using distributed Bragg reflectors to achieve an orthogonal geometry between the excitation laser and emission detection. The background noise is thought to come from the drift of the Michelson interferometer, which is used as a spectral filter, resulting in unintended detection of photons from the Rayleigh peak. The measured $g^{(2)}(0)$ value of 0.08 [Fig. 3(b)] is comparable but less than our simulation results: min $[g^{(2)}(0)]$ is 0.16 for the Gaussian filter, 0.22 for the rectangular filter, and 0.36 for the Lorentzian filter, in which parameters for the simulation are extracted from the report: $2\Omega_R = 53.8$ μeV, $\gamma_{sp} = 1$ μeV, and $\Gamma_{ph} = 3.5$ μeV. This discrepancy could be due to a difference in the spectral filter types; they used a pair of Michelson interferometers (each of which works as a sinusoidal filter) specially tailored to filter out two Mollow peaks irrelevant to the SP emission. Therefore, the direct comparison should be made with such a pair of sinusoidal filters, although it has remained as a future issue.

An interesting issue remaining will be extending this method to simulations for periodic and short-pulsed pumping, which will allow us to study the effect of the spectral filtering in case of short-pulse excitations aiming at more realistic operations of the QD SP source [14].

ACKNOWLEDGMENTS

We thank Y. Ota, M. Holmes, T. Rae, S. Kako, T. Miiyazawa, M. Yamaguchi, and T. Horikiri for useful comments and discussions. This work is supported by the Project for Developing Innovation Systems of the Ministry of Education, Culture, Sports, Science, and Technology. This work is also supported by Japan Society for the Promotion of Science KAKENHI Grant No. 15K20931.

[1] C. H. Bennett and G. Brassard, Quantum cryptography: Public key distribution and coin tossing, in *Proceedings of the IEEE International Conference on Computers, Systems and Signal Processing, Bangalore, India, 1984* (IEEE, New York, 1984), pp. 175–179; Quantum public key distribution system, IBM Tech. Discl. Bull. **28**, 3153 (1985).

[2] E. Waks, K. Inoue, C. Santori, D. Fattal, J. Vuckovic, G. S. Solomon, and Y. Yamamoto, Secure communication: Quantum cryptography with a photon turnstile, Nature (London) **420**, 762 (2002).

[3] S. Buckley, K. Rivoire, and J. Vučković, Engineered quantum dot single-photon sources, Rep. Prog. Phys. **75**, 126503 (2012).

[4] C. Santori, M. Pelton, G. Solomon, Y. Dale, and Y. Yamamoto, Triggered Single Photons from a Quantum Dot, Phys. Rev. Lett. **86**, 1502 (2001).

[5] K. Takemoto *et al.*, Transmission experiment of quantum keys over 50 km using high-performance quantum-dot single-photon source at 1.5 μm wavelength, Appl. Phys. Express **3**, 092802 (2010).

[6] S. Kako, C. Santori, K. Hoshino, S. Götzinger, Y. Yamamoto, and Y. Arakawa, A gallium nitride single-photon source operating at 200 K, Nat. Mater. **5**, 887 (2006).

[7] M. J. Holmes, K. Choi, S. Kako, M. Arita, and Y. Arakawa, Room-temperature triggered single photon emission from a III-nitride site-controlled nanowire quantum dot, Nano Lett. **14**, 982 (2014).

[8] T. Nakaoka, Y. Tamura, T. Miyazawa, K. Watanabe, Y. Ota, S. Iwamoto, and Y. Arakawa, Wavelength tunable quantum dot single-photon source with a side gate, Jpn. J. Appl. Phys. **51**, 02BJ05 (2012).

[9] D. Englund, D. Fattal, E. Waks, G. Solomon, B. Zhang, T. Nakaoka, Y. Arakawa, Y. Yamamoto, and J. Vučković, Controlling the Spontaneous Emission Rate of Single Quantum Dots in a Two-Dimensional Photonic Crystal, Phys. Rev. Lett. **95**, 013904 (2005).

[10] S. Strauf, N. G. Stoltz, M. T. Rakher, L. A. Coldren, P. M. Petroff, and D. Bouwmeester, High-frequency single-photon source with polarization control, Nat. Photon. **1**, 704 (2007).

[11] A. Muller, E. B. Flagg, P. Bianucci, X. Y. Wang, D. G. Deppe, W. Ma, J. Zhang, G. J. Salamo, M. Xiao, and C. K. Shih, Resonance Fluorescence from a Coherently Driven Semiconductor Quantum Dot in a Cavity, Phys. Rev. Lett. **99**, 187402 (2007).

[12] S. Ates, S. M. Ulrich, S. Reitzenstein, A. Löffler, A. Forchel, and P. Michler, Post-Selected Indistinguishable Photons from the Resonance Fluorescence of a Single Quantum Dot in a Microcavity, Phys. Rev. Lett. **103**, 167402 (2009).

[13] R. Hanbury-Brown and R. Q. Twiss, Correlation between photons in two coherent beams of light, Nature (London) **177**, 27 (1956).

[14] K. Kamide, S. Iwamoto, and Y. Arakawa, Impact of the Dark Path on Quantum Dot Single Photon Emitters in Small Cavities, Phys. Rev. Lett. **113**, 143604 (2014).

[15] E. del Valle, A. Gonzalez-Tudela, F. P. Laussy, C. Tejedor, and M. J. Hartmann, Theory of Frequency-Filtered and Time-Resolved N-Photon Correlations, Phys. Rev. Lett. **109**, 183601 (2012).

[16] E. del Valle, Distilling one, two and entangled pairs of photons from a quantum dot with cavity QED effects and spectral filtering, New J. Phys. **15**, 025019 (2013).

[17] A. Gonzalez-Tudela, F. P. Laussy, C. Tejedor, M. J. Hartmann, and E. del Valle, Two-photon spectra of quantum emitters, New J. Phys. **15**, 033036 (2013).

[18] C. Sanchez Munoz, E. del Valle, C. Tejedor, and F. P. Laussy, Violation of classical inequalities by photon frequency filtering, Phys. Rev. A **90**, 052111 (2014).

[19] A. Gonzalez-Tudela, E. del Valle, and F. P. Laussy, Optimization of photon correlations by frequency filtering, Phys. Rev. A **91**, 043807 (2015).

[20] J. D. Cresser, Intensity correlations of frequency-filtered light fields, J. Phys. B **20**, 4915 (1987).

[21] G. Nienhuis, Spectral correlations in resonance fluorescence, Phys. Rev. A **47**, 510 (1993).

[22] K. Joosten and G. Nienhuis, Influence of spectral filtering on the quantum nature of light, J. Opt. B **2**, 158 (2000).

[23] M. J. Clauser, Relaxation effects in spectra: Eigenvalue treatment of superoperators, Phys. Rev. B **3**, 3748 (1971).

[24] J. Wiersig *et al.*, Direct observation of correlations between individual photon emission events of a microcavity laser, Nature (London) **460**, 245 (2009).

[25] H. J. Carmichael, *Statistical Methods in Quantum Optics 1: Master Equations and Fokker-Planck Equations*, 2nd ed. (Springer, Berlin, 2003).

[26] M. Yamaguchi, T. Asano, K. Kojima, and S. Noda, Quantum electrodynamics of a nanocavity coupled with exciton complexes in a quantum dot, Phys. Rev. B **80**, 155326 (2009).

[27] S. Ritter, P. Gartner, C. Gies, and F. Jahnke, Emission properties and photon statistics of a single quantum dot laser, Opt. Express **18**, 9909 (2010).

[28] J. Johansen, S. Stobbe, I. S. Nikolaev, T. Lund-Hansen, P. T. Kristensen, J. M. Hvam, W. L. Vos, and P. Lodahl, Size dependence of the wavefunction of self-assembled InAs quantum dots from time-resolved optical measurements, Phys. Rev. B **77**, 073303 (2008).

[29] B. R. Mollow, Power spectrum of light scattered by two-level systems, Phys. Rev. **188**, 1969 (1969).

[30] T. Miyazawa, K. Takemoto, Y. Sakuma, Song Haizhi, M. Takatsu, T. Yamamoto, and Y. Arakawa, Suppression of multi-photon emission in 1.5-μm quantum-dot single-photon source, in *2013 International Conference on Indium Phosphide and Related Materials (IPRM), Kobe, Japan, 2013* (IEEE, 2013), pp. 1–2.

[31] S. Weiler, D. Stojanovic, S. M. Ulrich, M. Jetter, and P. Michler, Postselected indistinguishable single-photon emission from the Mollow triplet sidebands of a resonantly excited quantum dot, Phys. Rev. B **87**, 241302(R) (2013).